Bilecik Şeyh Edebali Üniversitesi Fen Bilimleri Dergisi
Bilecik Seyh Edebali University Journal of Science
12(1), 108-136, 2025

DOİ: 10.35193/bseufbd.1463785
e-ISSN: 2458-7575 (https://dergipark.org.tr/tr/pub/bseufbd)

Araştırma Makalesi - Research Article

Real-Time Control and Performance Analysis of PLC-SCADA Supervised Stand-Alone Solar Tracking Systems

PLC-SCADA Denetimli Bağımsız Güneş Takip Sistemlerinin Gerçek Zamanlı Kontrolü ve Performans Analizi

Faysil Alfirjani[1], Hüseyin Altınkaya[2*]

Geliş / Received: 03/04/2024 ***Revize / Revised: 05/07/2024*** ***Kabul / Accepted: 05/07/2024***

ABSTRACT

This paper presents the real-time control of single-axis and dual-axis solar tracking systems, as well as monitoring of a fixed solar panel system, using PLC (Programmable Logic Controller) and SCADA (Supervisory Control and Data Acquisition). The systems were designed using a novel tracking mechanism and a novel energy generation evaluation method. Based on their efficiencies as well as the power they produced, these three solar panel systems were compared accordingly. In all three systems, identical solar panels having 100 Wp power were used. To control both single-axis and dual-axis solar panels efficiently, an S7-1200 type PLC was employed. Real-time clock and astronomical data were used to control the axis angle of the PV panels. The system was comprehensively monitored and controlled in real-time through the implementation of PLC-SCADA software. The obtained data were recorded and displayed on SCADA screen, and were subsequently analyzed to determine the power output of the three panels under varying climatic conditions. The evaluation of the obtained results was made accordingly. In a total of 61-day period which encompassed 42 days of sunshine, 11 days of cloud and 8 days of rain, double-axis photovoltaic panel produced 337.34 Wh, single-axis photovoltaic panel generated 314.32 Wh and fixed photovoltaic panel produced 220.49 Wh on average. On daily average, double-axis photovoltaic panel produced 7.32% more energy as compared to single-axis photovoltaic panel and 52.99% more energy as compared to fixed photovoltaic panel, whereas single-axis photovoltaic panel produced 42.55% more energy than fixed photovoltaic panel.

Keywords- Solar tracking system, PLC, SCADA, Energy generation

ÖZ

Bu makalede, PLC (Programlanabilir Mantıksal Denetleyici) ve SCADA (Yönetimsel Denetim ve Veri Toplama) kullanılarak tek eksenli ve çift eksenli güneş takip sistemlerinin gerçek zamanlı kontrolü ve sabit bir güneş paneli sisteminin izlenmesi sunulmaktadır. Sistemler, yeni bir takip mekanizması ve yeni bir enerji üretimi değerlendirme yöntemi kullanılarak tasarlanmıştır. Bu üç güneş paneli sistemi verimliliklerine ve ürettikleri güce göre karşılaştırılmıştır. Her üç sistemde de 100 Wp gücünde özdeş güneş panelleri kullanılmıştır. Hem tek eksenli hem de çift eksenli güneş panelini etkili bir şekilde kontrol etmek için S7-1200 tip bir PLC kullanılmıştır. PV panellerinin eksen açısını kontrol etmek için gerçek zamanlı saat ve astronomik veriler kullanılmıştır. Sistem, PLC-SCADA yazılımının uygulanması yoluyla gerçek zamanlı olarak kapsamlı bir şekilde izlenmiş ve kontrol

[1] Contact: faysilal88@gmail.com (https://orcid.org/0000-0003-3130-2418)
Department of Electrical-Electronics Engineering, Karabuk University, 78050 Karabük, Türkiye
[2*] Corresponding Author Contact: haltinkaya@karabuk.edu.tr (https://orcid.org/0000-0003-1956-1695)
Department of Electrical-Electronics Engineering, Karabuk University, 78050 Karabük, Türkiye

edilmiştir. Elde edilen veriler kaydedilerek SCADA ekranında görüntülenmiş ve daha sonra değişen iklim koşulları altında üç panelin güç çıkışını belirlemek için analiz edilmiştir. Elde edilen sonuçların değerlendirmesi buna göre yapılmıştır. 42 gün güneşli, 11 gün bulutlu ve 8 gün yağmurlu olmak üzere toplam 61 günlük dönemde, çift eksenli fotovoltaik panel ortalama 337,34 Wh, tek eksenli fotovoltaik panel 314,32 Wh ve sabit fotovoltaik panel 220,49 Wh üretmiştir. Günlük ortalamada, çift eksenli fotovoltaik panel tek eksenli fotovoltaik panele göre %7,32 ve sabit fotovoltaik panele göre %52,99 daha fazla enerji üretirken, tek eksenli fotovoltaik panel sabit fotovoltaik panele göre %42,55 daha fazla enerji üretmiştir.

Anahtar Kelimeler- Güneş takip sistemi, PLC, SCADA, Enerji üretimi

I. INTRODUCTION

The global importance of clean and renewable energy has become increasingly apparent in recent times. Reduction of carbon emissions, achieved through the decreased usage of fossil fuel resources, is the primary objective for many countries across the globe. Reducing the use of fossil fuel resources will only be possible with the increase in energy production and efficiency of renewable and clean energy resources. Solar energy has an important place among renewable energy resources, and its share in electricity production has increased significantly in the last decade. In 2022, this share was found to be 4.5% in the world [1]. As of March 2024 in Turkey, the share of solar energy in power plants was 11.74% in terms of installed power and its share in total electricity production was 4.93% [2].

Solar power plants and solar farms can be set up on a larger scale using fixed photovoltaic (PV) panels. Some small powered systems, some medium sized solar power plants, and some experimental setups can either be designed as uniaxial or biaxial. Nowadays, single-axis or dual-axis panels are considered less cost-effective and feasible due to their high installation and maintenance costs. Consequently, solar energy systems are being installed on a massive scale, primarily utilizing fixed PV panels.

The amount and efficiency of the energy obtained from PV panels can be increased by cooling systems, maximum power point tracking (MPPT) algorithms and solar tracking systems (STSs) [3,4]. STSs are known as systems that are effectively designed in order to track sunlight in such a way to absorb the energy efficiently using PV panels. Solar tracking systems may be classified according to drive types, tracking strategies, control systems, and degrees set for movement [5-7].

Solar tracking systems (STSs) can be classified into two categories as, closed loop and open loop systems based on their control mode. In the closed loop tracking system; timely position of the sun is detected using sensors and the data obtained is returned as feedback. Using the feedback control, comparator or microprocessor can detect the errors in the system easily, thus sending the signals to motors for the correction of errors. Such a system runs on the principle of feedback control system. Considering this system to be a pre-defined algorithm or a passive system based mainly on calculations conducted for trajectory of sun, drive system used for tracker's movement is of secondary importance. In the open loop tracking system, a controller is used in order to give the motors a driving signal mainly based on the operating algorithm and the input data of the system alone. In terms of desired output, open loop tracking system does not have any characteristics regarding the output data observation or evaluation. Therefore, the implementation process of this system is relatively simple and cost-effective as compared to the closed loop tracking system. The open loop tracking system has no process involving rectification, therefore, the aim has to be achieved by algorithm alone [8].

STSs can be categorized into two main groups based on their driver types: Passive Solar Tracking and Active Solar Tracking. The former has no mechanical drives to rotate the PV panels towards the radiations of sun. However, either shape memory alloys or low boiling point compressed gas fluid are used in this system in order to move the panels angularly as well as to establish equilibrium after being exposed to an unbalanced illumination. Despite being effective and less complex, this system fails to function with higher efficiencies at some lower temperatures.

Nomenclature

A_V	Voltage gain, V/V
I_{MP}	Typical value of maximum power voltage, V
I_{SC}	Short circuit current of the PV panel, A
V_{MP}	Typical value of maximum power current, A
V_{OC}	Open circuit voltage of the PV panel, V
FF	Fill factor
P_{MP}	Maximum power of PV panel, W
R_f	Feedback resistance, Ω
R_i	Input resistance, Ω
W_{DPV}	Average amount of produced energy of DPV, kWh
W_{FPV}	Average amount of produced energy of FPV, kWh
W_{SPV}	Average amount of produced energy of SPV, kWh
η	Efficiency percentage of the PV panels (%)

Acronyms

DAPV	Double-Axis Photovoltaic Panel
FPV	Fixed Photovoltaic Panel
PLC	Programmable Logic Controller
SCADA	Supervisory Control and Data Acquisition
SAPV	Single-Axis Photovoltaic Panel
STS	Solar Tracking System

The later uses electrical drives and mechanical gear trains to move the panels to a point that is considered to be normal to the radiations of sun. This system uses sensors, microprocessors and motors in order to track solar trajectory and when compared with passive solar trackers, this system is known to be accurate and efficient. Such systems need to be powered as they consume energy [9].

The degree of movement determines the directions for an independent movement. Based on this, solar tracking systems may be classified as single-axis and dual-axis tracking systems. Parameters like longitude, latitude, solar azimuth angle, elevation angle, declination angle, incident angle and zenith angle play a vital role in determining appropriate locations and directions. In single-axis system, the movement tends to be in only one axis, and rotation is utilized to align the solar panel perpendicular to the incoming solar radiation. These trackers are known to be cheaper and less complex. However, when compared with dual-axis trackers, they are found to be less efficient. In dual-axis solar tracking system, the rotation tends to be in two axes and generally, the rotations are perpendicular. These trackers require more complex control systems and are efficient when compared with single-axis trackers [5,10].

According to the tracking strategy, STSs are divided into two main groups as sensor-based and sensorless. Solar Tracking System (STS) uses microprocessors and electro-optical sensors to detect the precise position of the sun. The microprocessor is initially fed with a signal, and subsequently, the motors are actuated through another signal from the microprocessor. Similar designs use DC motors with reduction gears, and sensors such as LDRs and electronic circuits for solar tracking system. The proposed systems use sensors, which give required inputs to electronic circuits, in order to actuate the motors. Time and Date type solar tracking systems only use pre-defined algorithms based on mathematical formulations calculating the sun's trajectory to determine the position of sun at a particular time interval and orient the PV panels accordingly. No feedback loop or sensor is involved in such a system. Hence, only algorithm plays the role in efficient working of the system. Solar tracking systems with Time, Date and Sensors work according to a predefined algorithm. They are used to check the overall operation conducted by sensors involved in the system, ensuring that the precise position of the sun is detected and that the panels are driven and oriented accordingly. A Dual-axis hybrid STS consisting of an open loop tracking system based on solar movement model and a closed loop tracking system based on feedback signals that are proportional to output power has been proposed for mixed tracking strategy [10].

The present study involves the real-time control of dual-axis, single-axis, and fixed PV panels. The STSs presented in this study are active, open-loop, driver type, and feedback sensorless systems, which do not require an external internet connection and are based solely on astronomical data such as date and time. By entering the surface azimuth angle and zenith angle values into data block in PLC software, the system can be operated anywhere in the world regardless of location. A novel structural design has been developed for dual-axis and single-axis solar tracking systems. The mechanical system designed for the PV panels allows for movement in both north-south (up-down) and east-west (right-left) directions. In order to provide these movements, worm gear reducers are used. The system can move 360 degrees and 180 degrees in east-west and north-south direction, respectively. In addition, the system is able to show both movements simultaneously. With these features, the

system differs positively from other solar tracking systems presented in the literature, as the limitations and weaknesses seen in its mechanical structures are eliminated. In conjunction with the novel structural design for dual-axis and single-axis solar tracking, a new method has been used to evaluate the energy generation performance. This approach enhances the accuracy and reliability of the obtained results, allowing for a more comprehensive understanding of the system's performance. In order to compare the energy produced by DAPV, SAPV and FPV, area under Power-time (P-t) curves were calculated. The integration method and trapezoidal rule were used to calculate the energy amounts accordingly. The obtained data were analyzed using MATLAB software. The integration process was conducted using the trapezoidal method, which utilizes the Trapz command available in MATLAB.

The biggest disadvantage of STSs designed using LDR sensors and other light-based sensors is the continuous variation in the intensity of light due to various reasons. This continuous variation is detected by the LDR sensor, leading to a constant change in the position of the solar panel. During conditions such as sunrise, sunset, rain, snow and fog, the system tends to orient towards the direction with the highest radiation, regardless of the direct incoming radiation. This may cause the system to remain in scanning mode to find the direction with the highest radiation and may require the motor to consume more energy for tracking. The sensors used in STS can be affected by environmental conditions over time and may produce inaccurate measurements. This can lead to incorrect detection of the sun's position or instability in the system. LDRs may deteriorate under high temperatures due to their structural sensitivity. Since LDRs are light-sensitive sensors, they can also be affected by artificial lighting during the day, which can result in power loss. Most of the photo sensors used in solar systems do not show a linear response under different temperatures and radiation values. The complexity and application costs of closed-loop LDR-based STSs are higher than those of open-loop systems. The disadvantages can be summarized as follows: stable operation only in open-air conditions - may not function properly in cloudy weather, higher energy consumption, high maintenance cost, and high price.

The designed system is free from the negative aspects of LDR-controlled solar tracking systems mentioned above and operates stably. The proposed automatic open-loop tracking system is not only cost-effective compared to closed-loop systems, but also provides greater accuracy, stability, and reliability than closed-loop systems in fluctuating weather conditions. Solar tracker based on date and time, which uses reduction gear units to move simultaneously in the east-west and north-south directions, has advanced accuracy with a tracking error of less than 0.2 degree, good motion stability, low maintenance costs, and easy installation. The system's reliability is enhanced by the inclinometer. Once the system is initially set up, it does not require manual alignment. By entering the surface azimuth and zenith angles based on the current coordinates, stable and reliable high solar energy harvesting efficiency can be achieved, regardless of the weather and the location. Another significant advantage of the system is that it does not require internet or GPS connectivity.

The rest of the paper is organized as follows: Literature review is presented in chapter 2. Some definitions of sun angles are given in chapter 3. In chapter 4, mechanical, electrical and software details of STSs, along with their design, installation and implementation, are given. In chapter 5, the results obtained are evaluated and discussed in detail. Finally, the conclusions have been provided in chapter 6.

II. LITERATURE REVIEW

A solar tracking system follows the position of the sun and keeps solar photovoltaic modules at the optimal angle to produce the maximum power output. This system offers benefits not only in terms of increased power and efficiency compared to fixed systems, but also plays a significant role in various solar energy applications, including economic analyses of large-scale solar energy projects. The idea behind designing a solar tracking system is to place solar photovoltaic modules in a position that can track the movement of the sun in order to capture the maximum amount of sunlight. Solar tracking system needs to be placed in such a way to take the best angle of incidence to maximize the electric power output. Several solar tracking principles and techniques have been proposed to efficiently track the sun. There are two main types of solar tracking systems depending on the degree of freedom of movement: single-axis solar tracking system and dual-axis solar tracking system. Various solar tracking systems such as single-axis tracking, dual-axis tracking, and single/dual-axis tracking have been evaluated in recent years. In the literature review given below, information on single-axis, dual-axis, single/dual-axis; sensor-based, sensorless; open loop, closed loop; and PID-fuzzy, image processing, real-time controlled STS is provided.

Jamroen et al. reported the design and implementation of an automatic dual-axis STS in their study [11]. The designed system aimed at adjusting the photovoltaic modules accurately. Using LDR logic design, the modules were oriented in primary and secondary axes in order to follow sun trajectory. In addition, a pseudo-azimuthal system was used in movement mechanism to achieve higher stability. Using a simple configuration method, LDRs were installed to eliminate tracking errors due to complex orientations. M. A. Jallal et al. developed an algorithm called DNNRODDPSO, based on machine learning, by hybridization of RODDPSO algorithm and

a novel neural network in order to predict the precise amount of produced energy. They used four dual-axis solar trackers in their system and the new combined system was called DAST system [12]. In a study, a single-axis tracker was designed by Y. Zhu et al. to enhance the overall solar radiation yield [13]. They used normal vector of tracked panels and analyzed the characteristics of the structure. Based on predicted model for solar radiation using geometrical relationship of sun and earth, their study was validated numerically.

Rousan AL et al. presented two efficient and intelligent single-axis and dual-axis STSs that were based on ANFIS [14]. The study confirmed that ANFIS can be used in design as well as implementation of STSs. The approach was successfully implemented during control of STSs. Orientation angle and optimum tilt values were predicted correctly and their simulation results showed high prediction rates and low mean square error rate.

Lim B et al. studied a large-scale industrial design of dual-axis tracker along with Multiple-Row-Elevation and Vertical axis Rotating Platform [15].

Based on tracking accuracy and energy gain, several studies presented evaluation techniques for STS types. In his analyses of solar resources on double axis tracking, Okoye [16] reported the yield to be high (1.86%-31.52%) when compared with single axis STS yield. Hence, based on results, the dual axis tracking was recommended. Only single axis STS was considered by Jacobson [17] and a comparison between V axis tracking and NS axis tracking was also provided. Usage of V axis tracking was suggested by him but it was not recommended to be used at higher latitudes. Performances of double axis tracking and fixed latitude tilt identical PV systems are theoretically and experimentally realized [18]. Martin [19] analyzed six PV plants that were installed in Spain and the complexity of dual axis trackers due to lack of maintenance were found during operation. By using an indicator, Bahrami et al. [20,21] combined the system's technical and economic feasibilities known as levelized-cost electricity. Their results showed that single-axis STSs could be more advantageous than dual-axis STSs in case of relatively lower installation cost for PV systems.

A real-time tracking algorithm was made by Antonanzas [22]. Under different weather conditions, the algorithm could maximize the production of energy. His results showed a 3.01% increase in solar radiation. In another study by Fernandez et al. [23], mathematical expressions for different single-axis STSs were presented. The models were based on some traditional approaches determining sun's position through global solar radiation. Barker et al. reported the dual-axis STS to have movements in two freedom degrees, thus tracking the sun easily in two different directions i.e. seasonal and daily motions [24]. Senturk and Eke [25] reported that dual-axis solar tracker was more accurate than single-axis STS while tracking sun trajectory. Another study by Roth et al. [26] showed that the output power of PV module may be increased up to approximately 33% as compared to the fixed PV module by using a dual-axis STS. Both single and double axes tracking systems can be classified as sensorless and sensor based solar.

In their study, Roth et al. [27] proposed an azimuth-altitude double-axis STS guided using closed loop control, and the tracker was fully automated. Batayneh et al. [28] proposed double-axis STS having altitude-azimuth mounting which is controlled by fuzzy controller. In different solar collector systems, solar tracker usage has been confirmed by previously conducted studies. Kacira et al. in Sanliurfa [29] reported average daily power gain of approximately 34.6% using double-axis STS when compared with fixed STS. Abdallah and Nijmeh [30] designed a double-axis STS for a PV system. It was reported that the system surface showed a 41.34% increase when compared with fixed surface. Abdollahpour et al. using image processing system, built a unique STS [31]. The system was based on relationship of opaque object with its shadow. According to their study, greater the angle between surface and object, longer will be the shadow if the surface is perpendicular to sunrays. And, if there is a 90^{o} angle, then no shadow will be casted on the surface.

In a study, Mavromatakis and Franghiadakis presented a novel single-axis tracker which could move plane of the collector in two directions through a special supporting structure [32]. Previous studies conducted on solar trackers show that they are used commonly in different solar collector systems. In a study, Chin et al. presented an active single-axis STS used in flat PV module systems [33]. The fuzzy logic controllers and conventional PI controllers were also compared in terms of performance. It was shown that at various optimum operating points, fuzzy logic controllers had better track capabilities and were faster [34]. H.-C. Lu and T.-L. Shih [35] presented fuzzy controlled dual-axis STS design having a maximum power point tracking. Proposed dual-axis STS design helps in improving the photovoltaic cell efficiency by tracking the sun. This mechanism has mainly two motors that allow the rotation of shafts to hold the PV panels in the optimum position.

A dual-axis STS based on real-time image processing and photo sensor was proposed in a study [36]. Dual axis solar tracker with satellite compass and inclinometer automatic positioning and tracking work was carried out [37]. A manual tracking mechanism was designed for a solar-powered steam injera stove [38].

The literature reveals that various configurations have been used in studies related to STS, including different mechanical setups, solar tracking methods (single or dual), solar tracking modes (active, passive,

manual), and solar tracking types (azimuth, azimuth-elevation, horizontal, vertical, etc.), as well as sensor-based and sensorless systems. Different configurations have been proposed in terms of hardware and software, considering cost, efficiency, and reliability. The literature provides recommendations for the most suitable configuration based on these factors.

In the studies found in the literature, generally only two PV systems (single-dual, single-fixed or dual-fixed) have been compared. In this study, however, three different PV systems, namely fixed, single-axis and dual-axis, have been compared. The mechanical installations in the literature have some weaknesses in terms of rotation angle, mechanical durability and operational flexibility. This study compares three different PV systems, including fixed, single-axis, and dual-axis systems. The system allows for two-directional movement (east-west and north-south) and provides a wide range of motion up to 360° in the east-west direction and 180° in the north-south direction. The system is based on astronomical date and time, eliminating the instability problem commonly observed in LDR systems. The system does not require internet or GPS, providing advantages in terms of cost and reliability. The reliability of the system is further enhanced by the inclinometer. Once the system is initially set up, it does not require manual alignment. The system can work regardless of the geographic location and weather conditions. A detailed comparison of the three systems was conducted based on measurements taken over 61 days under different weather conditions.

III. SUN ANGLES

Efficient utilization of solar energy requires knowledge of certain angles that exist between sun rays and earth surfaces. These angles include Latitude Angle, Declination Angle, Hour Angle, Tilt (Inclination) Angle, Zenith Angle, Elevation Angle, Azimuth Angle, Surface Azimuth Angle, and Incidence Angle. Among these, Tilt (Inclination) Angle, Zenith Angle, Azimuth Angle, and Surface Azimuth Angle are used in this study. Solar panels need to be adjusted according to these angles in order to track the solar position and utilize solar energy in the most effective way.

A. Tilt (Inclination) Angle

The tilt angle, represented as (β), refers to the angle between an inclined panel and the horizontal plane. Its orientation differs in the Northern and Southern Hemispheres, with north orientation in the Southern Hemisphere and south orientation in the Northern Hemisphere. This angle can range from 0º to 180º. By adjusting the panel's plane on the east-west horizontal axis with a single daily rotation, the tilt angle of that surface can be fixed for the day [5-7,39-41]. Equation 1 can be used to calculate the tilt angle.

$$\beta = | \Phi - \delta | \quad (1)$$

On the other hand, if the panel's plane is rotated continuously on the east-west horizontal axis, the tilt angle can be determined using equation 2, given as follows;

$$\tan \beta = \tan \theta_z \,.\, |\cos \gamma_s| \quad (2)$$

Similarly, if the plane is rotated around the north-south horizontal axis with continuous adjustments, the tilt angle of that surface can be determined using the equation given below:

$$[\tan \beta = \tan \theta_z \,.\, | \cos (\gamma - \gamma_s) | \quad (3)$$

Figure 1 shows the inclination (tilt) angle.

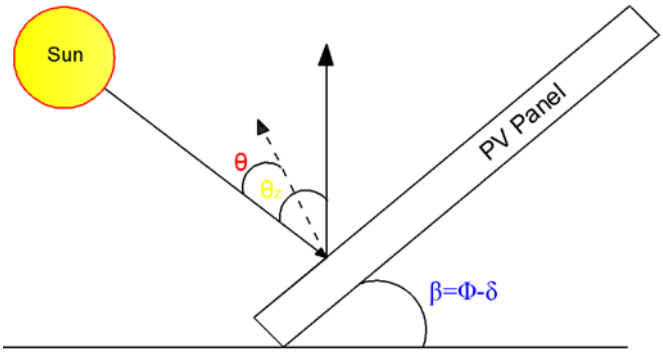

Figure 1. Inclination angle [41].

B. Zenith Angle

The angle between the line to the sun and the vertical axis is known as the zenith angle (θ_z). The surface of the earth has certain fundamental solar angles that are illustrated in Fig. 2. The zenith angle is 90 degrees at sunrise and sunset, while it is 0 degrees at noon. Some other angles are used to calculate this angle [5-7,40].

C. Azimuth Angle

Solar azimuth angle (γs) refers to the angle between the direction of direct solar radiation and the south or north position of the sun. The angle is positive when measured from south to west and negative when measured from south to east. At noon, the angle is 180 degrees. [5-7,39] This angle can be calculated using the following equation:

$$\gamma_s = \cos^{-1}\left[(\sin(\alpha)\,.\,\sin(\Phi) - \sin(\delta) \,/\, \cos(\alpha).\cos(\Phi)\right] \quad (4)$$

Figure 2 shows the Zenith angle, and the Azimuth angle.

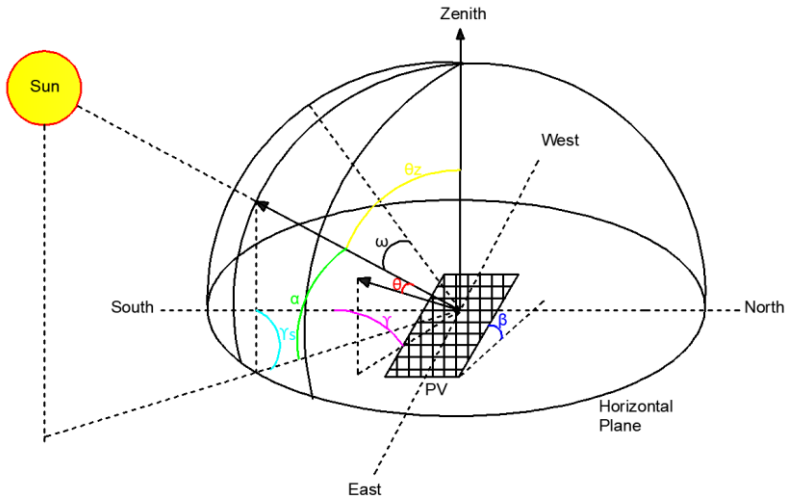

Figure 2. Basic solar angles [41].

D. Surface Azimuth Angle

The surface azimuth angle (γ) is the angle between the projection of the normal to the surface on a horizontal plane and the due south line. It is 0 when the surface faces south, positive (+) when it faces west, and negative (-) when it faces east. This angle can vary between -180 degrees and +180 degrees [5-7,39].

IV. SOLAR TRACKING SYSTEM DESIGN

In this study, three PV panels having a power of 100 watt (W) each were installed using three different setups, thus controlling single-axis STS and dual-axis STS movement. The short circuit current (I_{sc}) and open circuit voltage (V_{oc}) of the systems were carefully measured and then the current and voltage values were recorded at 10-minute intervals. In these systems, charging units, inverters and load resistors were not used. Furthermore, MPPT (maximum power point tracking) was not conducted. The stages comprising production and design, and hardware and software of three system prototypes (single axis panels, fixed panels and dual axis panels) have been explained in this part of the study.

A. Mechanical Part Design

Mechanical setups were designed to support and adjust the position of polycrystalline solar panels with 670 x 970 x 25 mm dimension and a power output of 100 watts peak (Wp). The default data of the solar panels is provided in Table 1.

Table 1. Solar panels datasheet.

Brand Name	Lexron
Model Type	LXRN100P
Electrical Characteristics	
Power Tolerance Range	5%
Rated Maximum Power (Pmax)	100Wp
Typical value of V_{oc}	22.10 V
Typical value of I_{sc}	6.45 A
Typical value of Maximum Power Voltage (V_{mp})	18.00 V
Typical value of Maximum Power Current (Imp)	6.11 A
Max. Series Fuse Rating	10.0A
Max. System Voltage	1000 V
Typical Weight	8.5 Kg
Module Class	Class A

Photovoltaic panels were placed on mechanical supports constructed using profiles. The mechanical system adjusts fixed panel's inclination angle between 30-60 degrees. The inclination angle to be considered in Karabük is found to be 39 degrees and in this study, the panel was fixed at this angle. The fixed panel has been shown in Figure 3.

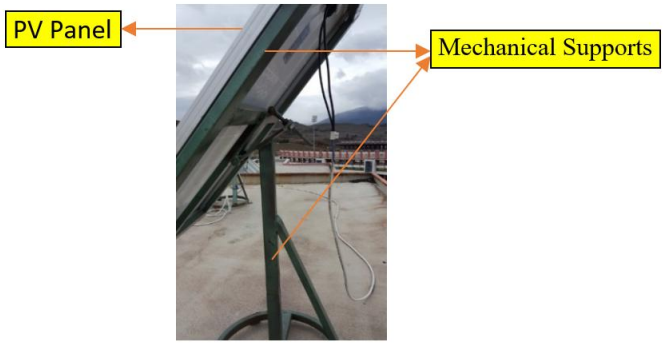

Figure 3. Fixed (flat) PV panel (FPV).

The mechanical system of single axis panel was designed in such a way to move in east-west direction. This movement was provided by the worm gear reducer. Stepper motor's torque was increased by decreasing revolution per minute (rpm) using the reducer. S30 type reducer was used in the system and its gear ratio was found to be 1:50. The designed mechanical system provided the capability to move 360 degrees. The mechanical system using reducer is found to be expensive as compared to systems using linear actuators. However, it provides more precise and broader movement. Single axis solar panel has been shown in Figure. 4.

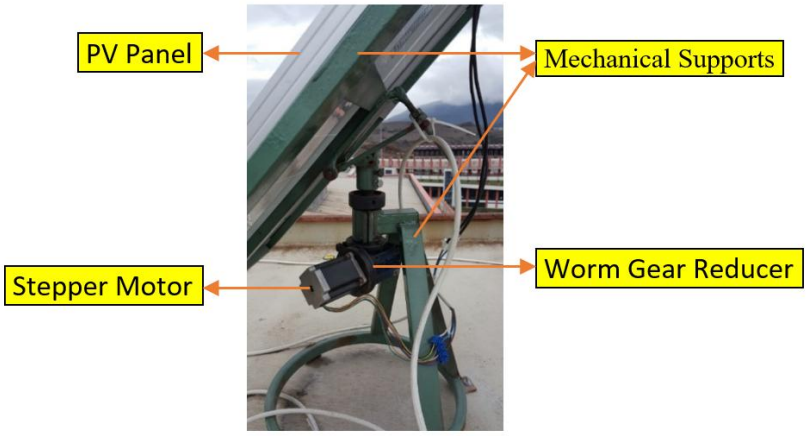

Figure 4. Single-axis PV panel (SAPV).

The mechanical system designed for dual-axis PV panel provided movements in north-south (up-down) and east-west (right-left) directions. In order to provide these movements, two worm gear reducers were used. The system showed 360 degree and 180-degree movements in east-west and north-south direction, respectively. In addition, the system was able to show both movements simultaneously. The dual-axis solar panel is shown in Figure 5.

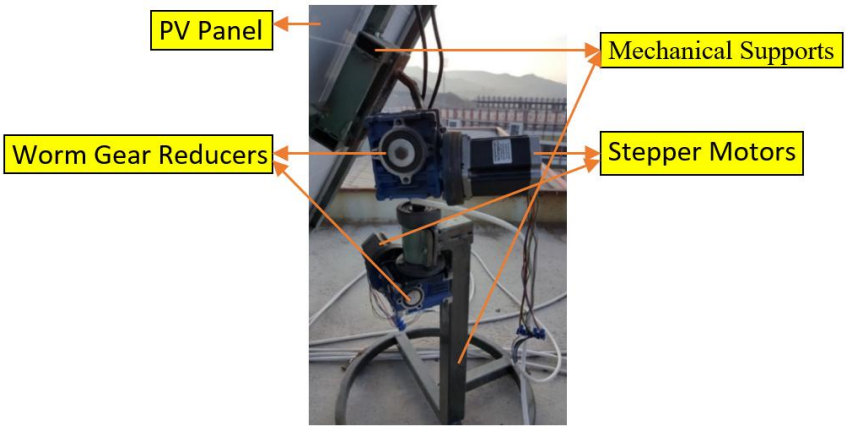

Figure 5. Dual-axis PV panel (DAPV).

B. Electrical Equipments

1) PLC (Programmable Logic Controller): Single-axis, dual-axis and fixed STSs were controlled and monitored remotely using S7-1200 PLC (1215C DC/DC/DC). Figure 6 shows the PLC used in this study having 2 analog outputs (AO), 2 analog inputs (AI), 10 digital outputs (DO), 14 digital inputs (DI) and 2 PROFINET ports. In addition, it has 125 KB memory.

Figure 6. S7-1200 PLC (1215C DC/DC/DC).

2) Current Measuring Unit: To accurately measure the current (I) of the panels, a circuit was required as the AI of PLC functions between 0-10 V or 0-20 mA. The short circuit current (I_{sc}) of photovoltaic panels were measured to be 6.45A. Printed circuits were made using Proteus/ISIS to measure the PV panel current using PLC as shown in Figure 7.

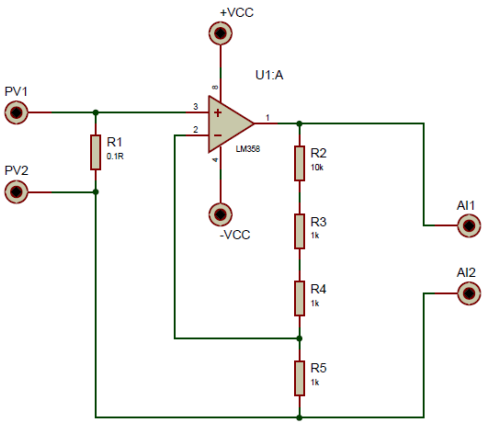

Figure 7. Current measuring circuit.

A non-inverting Op-Amp type ‘LM 358’ was used in this circuit. Gain formula for the Op-Amp can be given as:

$$A_v = 1 + \frac{R_f}{R_i} \quad (5)$$

Where; A_v is voltage gain (V/V), R_f and R_i are feedback resistance (Ω) and input resistance (Ω), respectively. The resistance values for R_f and R_i were 12 KΩ and 1KΩ respectively, in the printed circuit. The calculations using the given formula (1) yield the voltage gain (A_v) to be 13.

The output of panels was connected to resistors having 0.1Ω values. Using the Op-Amp connected to analog inputs of PLC, voltage on these resistors was increased. Considering analog input max. voltage as 10V (6.45x0.1x13=8.39V) and I_{sc} current of PV panels as 6.45A, the gain was found to be 13. Accordingly, the codes were written in ladder logic in the PLC software. Figures. 8 and 9 show the printed circuit's top and bottom view, respectively.

Fig.ure 8. Printed circuit for current measurement (Top view).

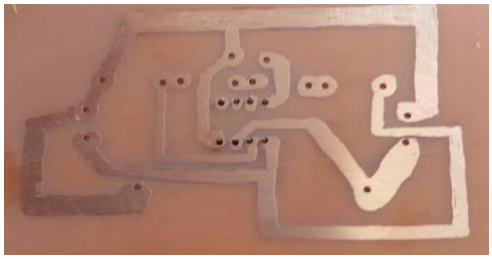

Figure 9. Printed circuit for current measurement (Bottom view).

3) Current Measuring Unit: Voltage measurement of PV panels is performed using AIs, and AIs run on 0-10 V. Therefore, a voltage divider was required in the study. V_{oc} voltage of given panels was found to be 22.10V. To measure the PV panels' voltage using PLC, the Proteus/ISIS printed circuit given in Figure 8 was designed. Using this circuit, voltage measurement was conducted for up-to 30V and the codes were written accordingly using PLC software (30Vx (10K/30K)=10V). Figure 10 shows the voltage measuring circuit's Proteus/ISIS scheme, and Figures 11 and 12 show the printed circuit's top and bottom view, respectively.

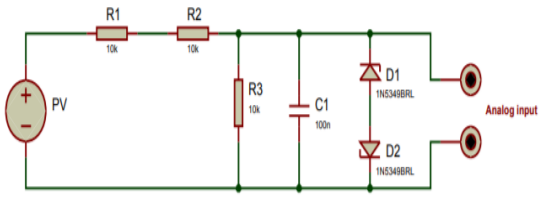

Figure 10. Voltage measuring circuit.

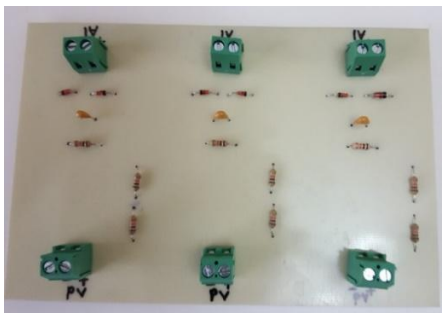

Figure 11. Printed circuit for voltage measurement (Top view).

Figure 12. Printed circuit for voltage measurement (Bottom view).

An electrical enclosure was used in order to place the electrical equipment mentioned above and the cable connections of the equipment were made. The dimension of electrical enclosure was 500x700x200 mm (WXHXD) and the enclosure was made up of polyester. Figure 13 shows the electrical enclosure.

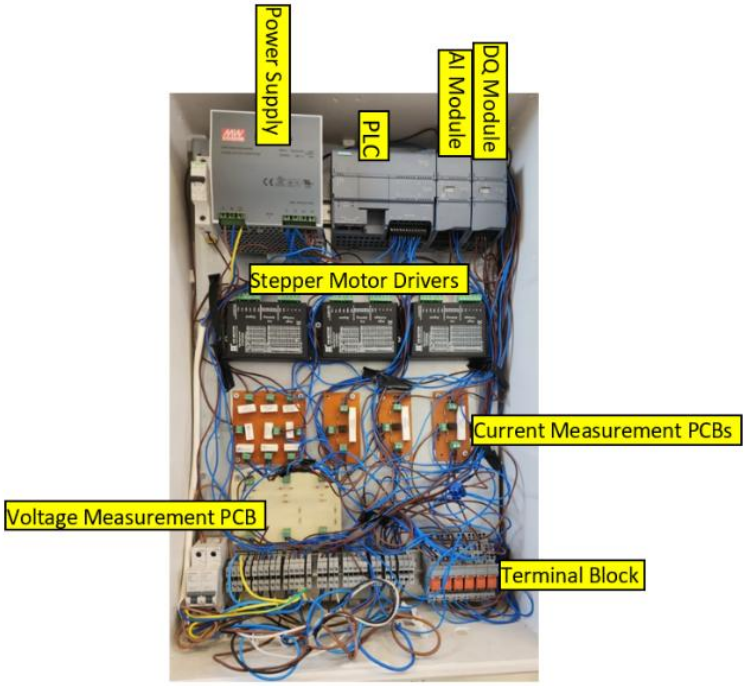

Figure 13. Electrical enclosure.

C. PLC and SCADA Software

TIA Portal V15 was used for providing an interface for PLC and SCADA software implementation. In this study, 1215C DC/DC/DC Siemens PLC was used, and ladder logic was preferred for programming. Using SIMATIC HMI Application and Win CC RT Advanced, PC screen was selected as operator panel instead of a real HMI panel. "Portal View" and "Device & Networks" of the TIA Portal Project, thus created, are shown in Figures 14 and 15, respectively.

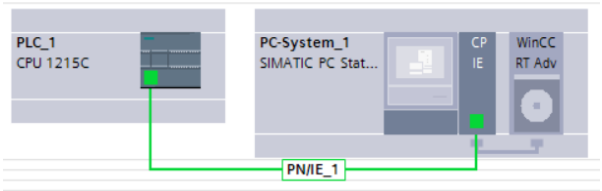

Figure 14. Device & Networks view.

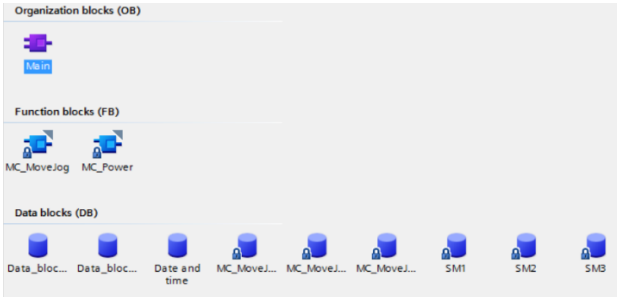

Figure 15. Portal view.

The PLC used in this study has 10 digital outputs (DQ) and 2 analog inputs (AI). Since a total of 15 DQs and 8 AIs were needed, 1 SM 1222 DQ module having 8 channels and 1 SM 1231 AI module having 8 channels were added. "Device Configuration view" has been shown in Figure 16.

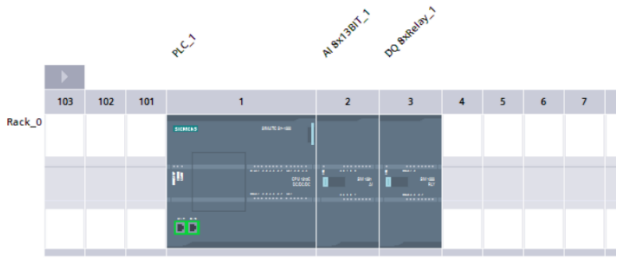

Figure 16. Device configuration view.

The voltage and current values of all three panels (SPV, DPV and FPV) were measured using AIs, and to drive the stepper motors and to control the relays, DQs were used. After the analog and digital hardware connections, TIA Portal interface was used to carry out the required software and hardware configurations. In order to drive the stepper motors, TO_PositioningAxis was used in programming of the software. In this study, the SPV was moved by stepper motor in east-west direction, whereas DPV was moved by two stepper motors in east-west as well as north-south directions.

Based on surface azimuth angle and elevation angle, east-west and north-south movements were adjusted, respectively. In order to provide axial movements to the panels, worm gear reducers were used in this study instead of the commonly used linear actuators. The use of worm gear reducers offers significant advantages in terms of adjusting the rotation angle over wide and clear ranges, as well as providing high movement sensitivity. However, it should be noted that the cost and workmanship associated with using worm gear reducers may be perceived as disadvantageous when compared to other methods. In order to direct the DPV in north-south and east-west directions, three worm gear reducers have been used in the designed system presented in this study. With north-south orientation, the slope angle of the DPV was adjusted, whereas with east-west orientation; based on the change in east-west angle, the panel's surface azimuth angle was found to be varying. This allowed for the necessary sun tracking to be achieved.

The astronomical solar data were used to control the system. The required data were accessed using 'https://midcdmz.nrel.gov/solpos/spa.html' website. After data entry regarding time zone, location coordinates of GTS, altitude of location to sea level, intervals in order to calculate the angles and desired date intervals etc., the website calculates the data and presents them in the form of list. The coordinates of Engineering Faculty building of Karabük University were entered in this interface, and data for the year 2020 were obtained at 10-minute intervals in excel file format. The data obtained comprised Surface azimuth angle, Azimuth angle, Zenith angle, Clock angle and Elevation angle. As an example, the data obtained between 13:00 and 15:00 hours on 18th of August, 2021 have been shown in Table 2.

Table 2. Data obtained for 18th August, 2021 between 13:00 and 15:00 hours.

Date	Time	Zenith Angle	S Azimuth Angle
8.18.2021	13:00:00	28.280655	3.505400
8.18.2021	13:10:00	28.481531	8.614443
8.18.2021	13:20:00	28.846818	13.637170
8.18.2021	13:30:00	29.370236	18.529488
8.18.2021	13:40:00	30.043310	23.255493
8.18.2021	13:50:00	30.855974	27.788647
8.18.2021	14:00:00	31.797193	32.111835
8.18.2021	14:10:00	32.855531	36.216538
8.18.2021	14:20:00	34.019618	40.101485
8.18.2021	14:30:00	35.278495	43.771078
8.18.2021	14:40:00	36.621849	47.233849
8.18.2021	14:50:00	38.040148	50.501093
8.18.2021	15:00:00	39.524698	53.585750

The rooftop of the Engineering Faculty building, located at Karabük University, was chosen as the appropriate site for the installation of the STSs. The faculty building coordinates were accessed from https://www.google.com/maps/place. In Figure. 17, the PV panels installed on the roof have been shown.

Figure 17. PV panels installed on rooftop.

The surface azimuth angle was used to adjust east-west movement of both single and dual-axis panels, whereas elevation angle was used to adjust the north-south movement of double-axis panel. In TIA portal interface, a data block was first created and then data related to the afore-mentioned two parameters were transferred to the data block created from the excel file. The DPV and SPV were kept at reference points during night hours. During daytime, the elevation angle and surface azimuth angle were obtained from relevant data blocks according to the date and time and the panels were brought and adjusted to these angles using stepper motors. After every 10 minutes interval, these processes were repeated. The number of moves or pulses of stepper motors, thus corresponding to movement degrees of mechanical system at the initial system setup, was determined by measurements and experiments. In the mechanical system, the gear ratio of worm gear reducer was 1/50. After every 10 minutes interval, the V_{oc} voltage and I_{sc} current of the installed panels were measured simultaneously. There was only 1 second interval between voltage and current measurements. The current and voltage values thus measured were displayed on supervisory control and data acquisition (SCADA) screen. Furthermore, the values were recorded using SCADA data logger. The collected data were utilized to plot and compare the performance of the PV panels. Figure 18 shows the flow chart of the system.

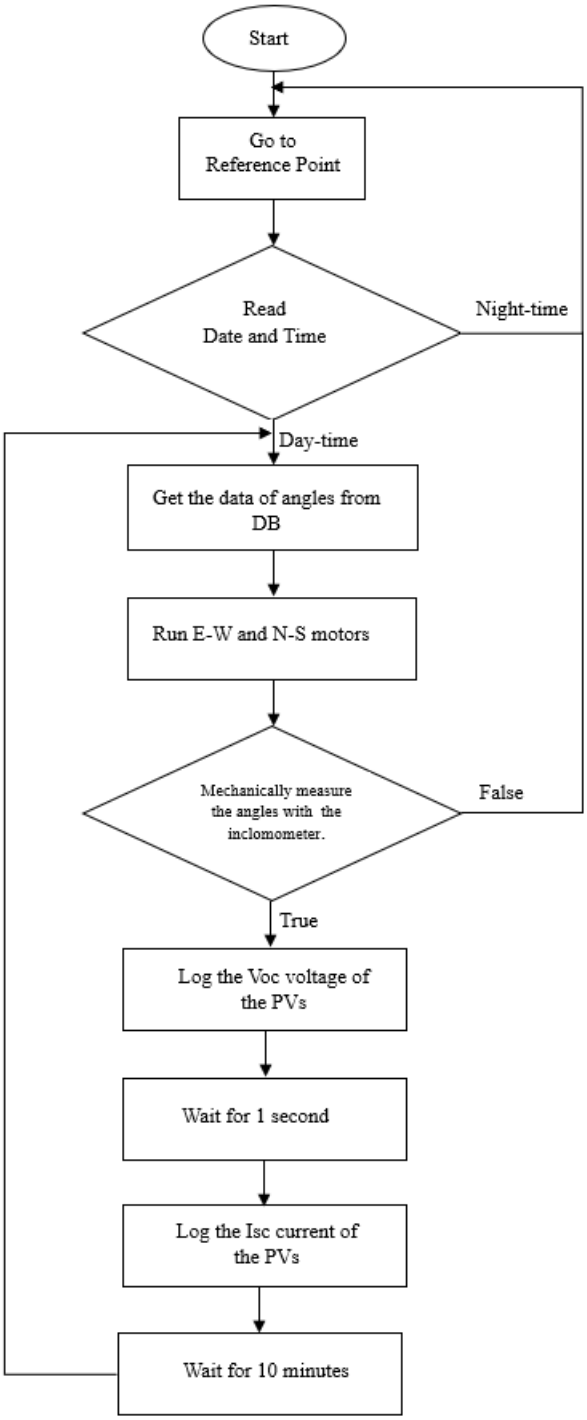

Figure 18. Flow chart of the system.

Part of the ladder diagram (software) is given in Appendix B. The block diagram of the system is shown in Figure 19.

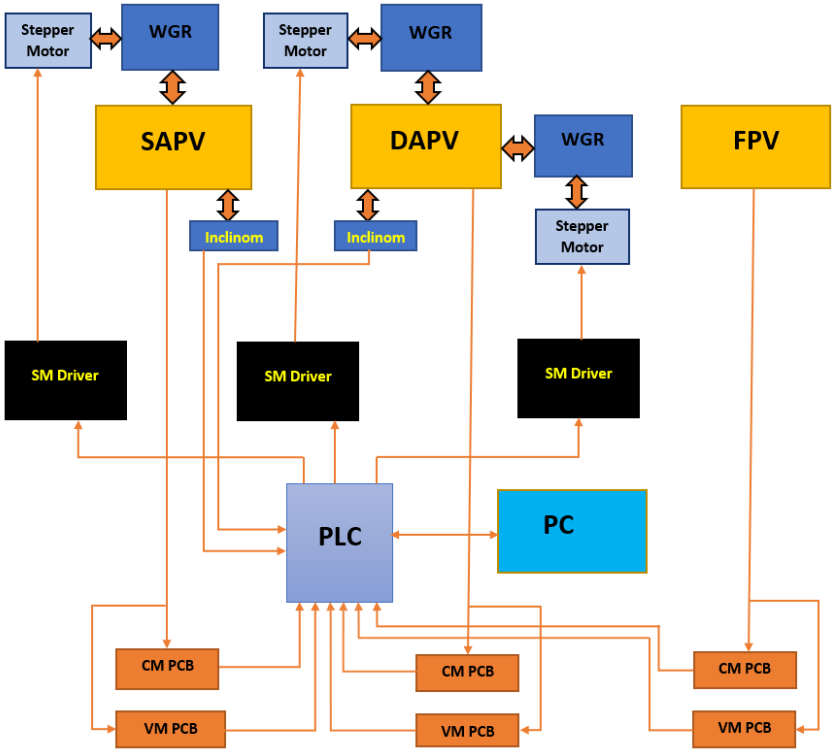

Figure 19. Block diagram of the system.

The system was monitored as well as controlled remotely using the developed SCADA software. A computer screen was used to monitor the SCADA output and meanwhile 3 SCADA screens were programmed. SCADA screen 1, regardless of date and time, shows the tools which can control the axis movements of panels manually. SCADA screen 1 has been shown in Figure 20.

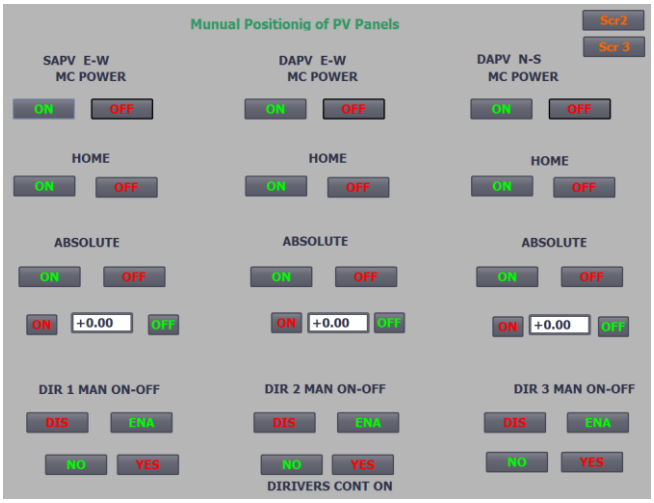

Figure 20. SCADA Screen 1.

In SCADA Screen 2 given in Figure 21, zenith angles and surface azimuth are displayed after every ten minutes in real time, and position data of stepper motors are provided accordingly.

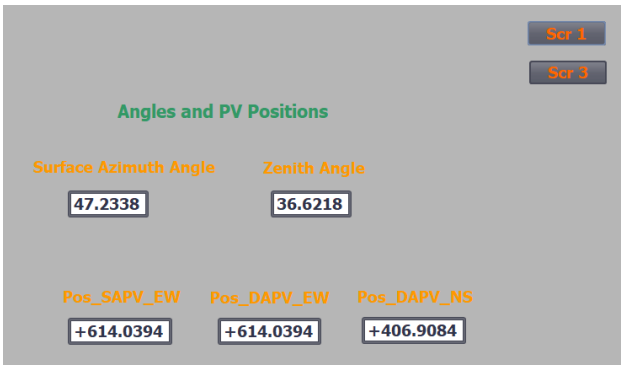

Figure 21. SCADA Screen 2.

In SCADA screen 3 shown in Figure 22, I_{sc} current and V_{oc} voltage of the panels are displayed. The values are recorded after every 10-minute intervals. The graphs are drawn and the operating characteristics of panels are analyzed. In addition, voltage and current values are obtained manually at any time interval.

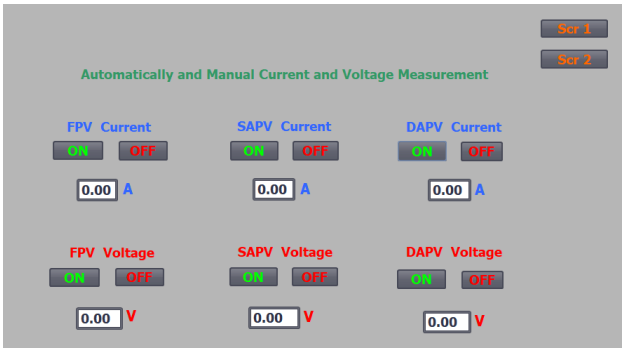

Figure 22. SCADA screen 3.

PV voltage was measured every 10 minutes, while the PV current was measured every 1 second. Figures 23 and 24 show current and voltage values of three panels measured at 14:40 on 18th August, 2021, respectively.

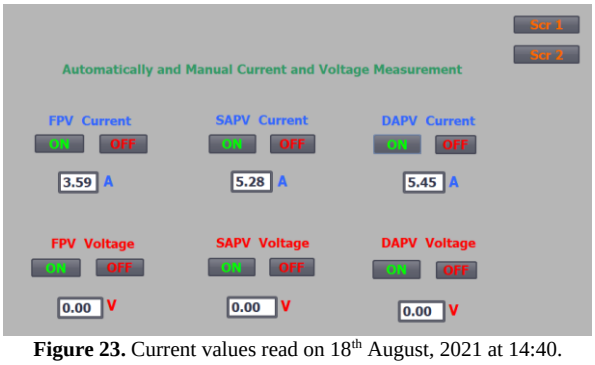

Figure 23. Current values read on 18th August, 2021 at 14:40.

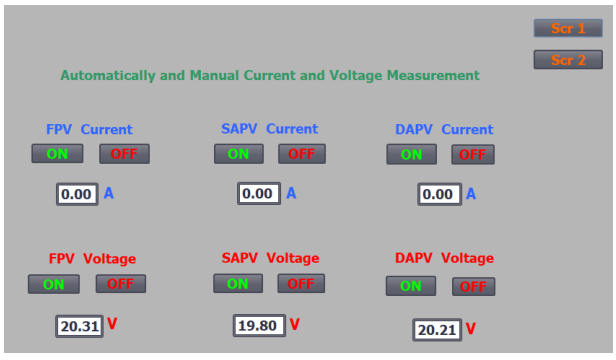

Figure 24. Voltage values read on 18th August, 2021 at 14:40.

The characteristic graphs of PV panels drawn using the real data recorded in the field have been presented in section 5.

D. Cost Analysis

Since this study is for experimental purposes and non-commercial, cost has been kept of secondary importance. Although relatively less costly studies are found in the literature, the increase in cost has been ignored in order to increase the robustness and reliability of the system. In Table 3, the costs of the installed FPV, SAPV and DAPV systems are given as a comparison.

Table 3. Cost of the PV systems.

Equipment	Unit Cost (USD)	FPV	SAPV	DAPV
PV Panel	70	1	1	1
Stepper Motor	30	-	1	2
Driver	40	-	1	2
Worm Gear Reducer	80	-	1	2
Mechanical Profiles	50	1	1	1
Total cost (USD)		120	270	420

The cost of SAPV is $150 (225%) more than the cost of FPV, and the cost of DAPV is $300 (350%) more than the cost of FPV.

In the 61-day period, DAPV produced 337.34 Wh, SAPV produced 314.32 Wh and FPV produced 220.49 Wh on daily average. On daily average, DAPV produced 7.32% more energy than SAPV and 52.99% more energy than FPV, and SAPV produced 42.55% more energy than FPV.

Although the cost of SAPV was 225% more than FPV, it was able to produce 43% more energy on a daily average. Although the cost of DAPV was 350% more than FPV, it was able to produce 53% more energy than FPV. According to these data, SAPV and DAPV do not seem profitable and feasible in terms of cost. It is seen that the costs will increase even more when the replacement of the equipment used in case of possible malfunction and maintenance fees are taken into consideration. Commercial, large powerful solar power plants are installed as FPV. Today, the average depreciation period of solar power plants is calculated as approximately 5 years. It is understood that in the proposed system, the depreciation period of SAPV and DAPV going to be much longer than 5 years compared to FPV.

V. MEASUREMENT RESULTS AND DISCUSSIONS

After every 10 minutes, the short circuit current (I_{sc}) and open circuit voltage (V_{oc}) of the three panels were automatically saved in .xlsx format using the StartLogging function available in TIA Portal, as well as using historical data. Table 4 displays the values that were measured at 14:41 and 14:51 on August 18, 2021.

Table 4. Measured values.

VarName	TimeString	VarValue
DAPV_voltage	18.08.2021 14:41	20.19844
SAPV_voltage	18.08.2021 14:41	19.7986
FPV_voltage	18.08.2021 14:41	20.30707
DAPV_current	18.08.2021 14:41	5.447847
SAPV_current	18.08.2021 14:41	5.279398
FPV_current	18.08.2021 14:41	3.592046
DAPV_voltage	18.08.2021 14:51	20.28347
SAPV_voltage	18.08.2021 14:51	19.88835
FPV_voltage	18.08.2021 14:51	20.42426
DAPV_current	18.08.2021 14:51	5.410903
SAPV_current	18.08.2021 14:51	5.25625
FPV_current	18.08.2021 14:51	3.386072

After arranging the obtained data, P-t, I-t and V-t graphs of relevant PVs were plotted using MATLAB program. Considering the fill factor (FF), the following formula was used to find the power (P).

$$FF = \frac{I_{MP}\, xV_{MP}}{I_{SC} xV_{OC}} \tag{6}$$

Where, maximum power current is denoted by I_{MP}, maximum power voltage is denoted by V_{MP}, and I_{SC} and V_{OC} are the short circuit current and open circuit voltage, respectively. As given in Table 1, the fill factor of the PV panels was found to be 0.7715. Power is calculated using formula 3 as follows.

$$P_{MP} = FFxI_{SC}xV_{OC} \tag{7}$$

The measurements taken between 1st of August, 2021 and 31st of September, 2021 are given as an instance along with the corresponding charts for three different days - 18th of August (sunny day), 21st of September (rainy day) and 25th of September (cloudy day). Voltage-Time (V-t), Current-Time (I-t) and Power-Time (P-t) graphs plotted for 18th August (sunny day) are given in Figures 25, 26 and 27, respectively.

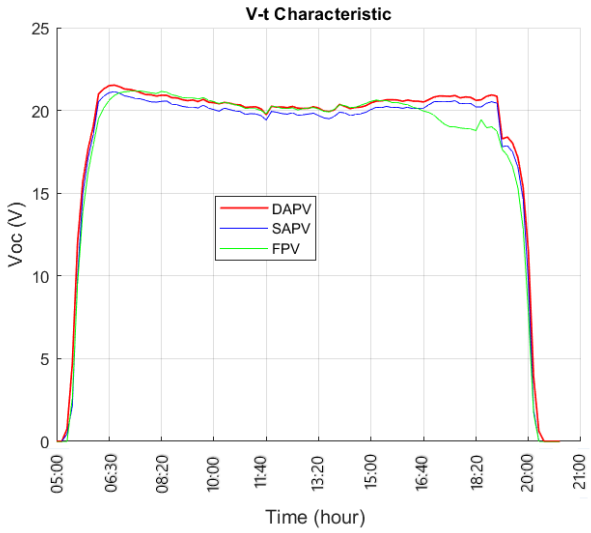

Figure 25. V-t graph plotted on 18th August, 2021.

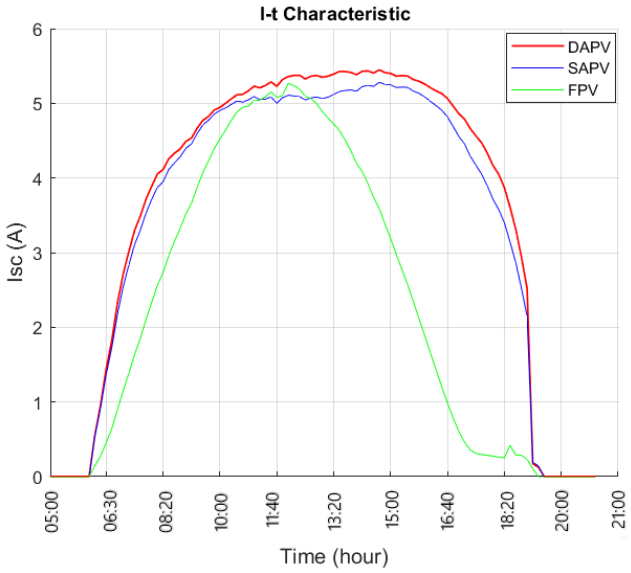

Figure 26. I-t graph plotted on 18th August, 2021.

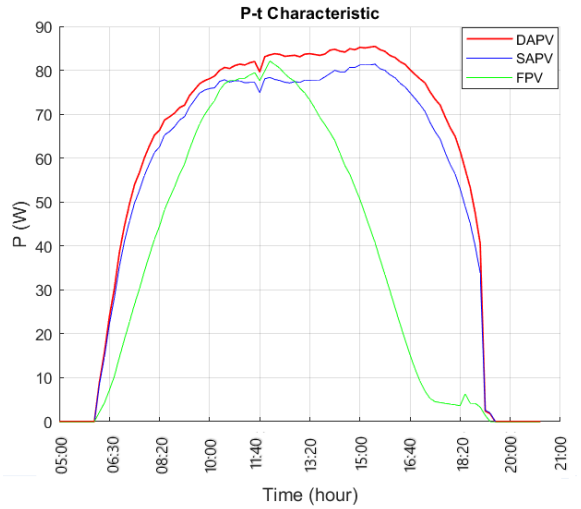

Figure 27. P-t graph plotted on 18th August, 2021.

Examining the three graphs, the voltage values of PV panels were observed to be much closer to each other throughout the day, whereas power and current values of PVs were found to be relatively close between morning and noon time. In the afternoon, the power and current of SAPV and DAPV were found to be increased significantly when compared with FPV. This is considered to be related to surface temperatures of PV panels and low activity of sun during morning hours.

Voltage-Time (V-t), Current-Time (I-t) and Power-Time (P-t) graphs plotted on 25th September (cloudy day), are given in Figures 28, 29 and 30, respectively. When the graphs were analyzed, the difference was not significant between PV panel voltages during the day, whereas there were significant differences observed in power and current values. Differences between power and current values of solar panels were seen to be decreased considerably during the times when sun disappeared.

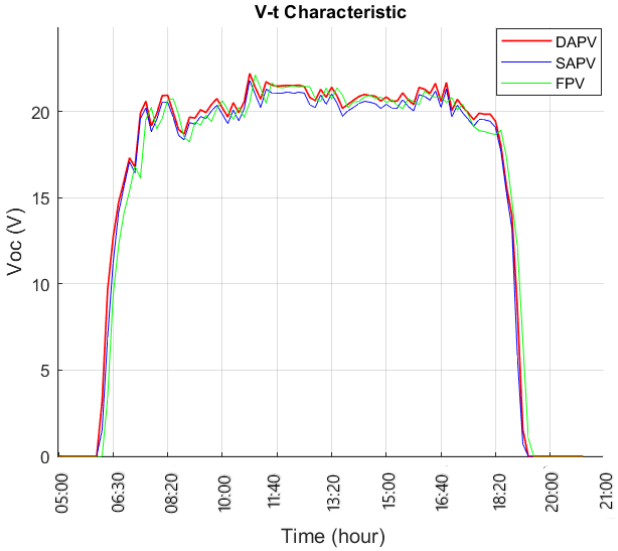

Figure 28. V-t graph plotted on 25th September, 2021.

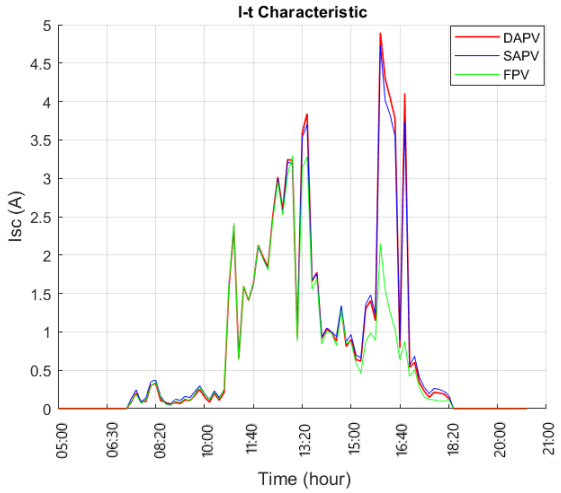

Figure 29. I-t graph plotted on 25th September, 2021.

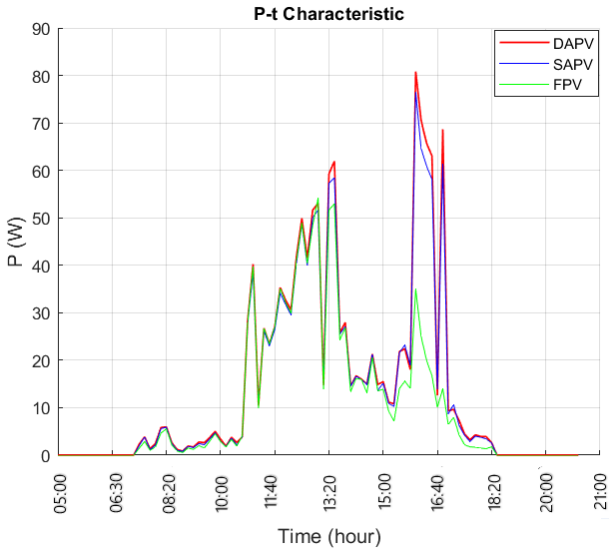

Figure 30. P-t graph plotted on 25th September, 2021.

Voltage-Time (V-t), Current-Time (I-t) and Power-Time (P-t) graphs plotted on 21st September (rainy day) are given in Figures 31, 32 and 33, respectively. Similar to the graphs above, the voltage values of the solar panels were found to be very close to each other, whereas, current and power values were also observed to be close to each other except when the sun did not disappear.

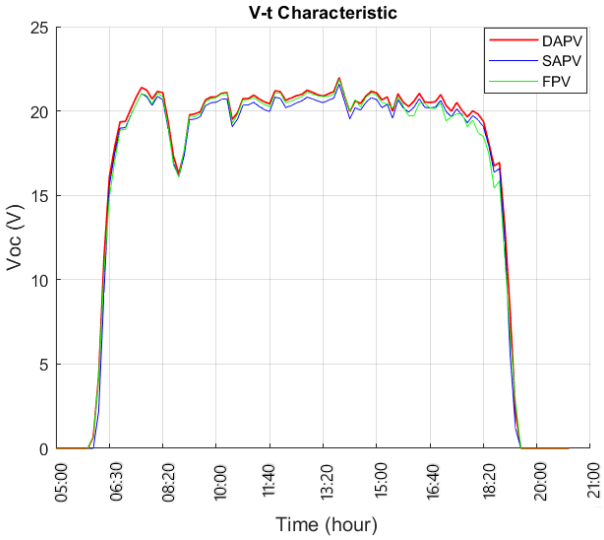

Figure 31. V-t graph plotted on 21st September, 2021.

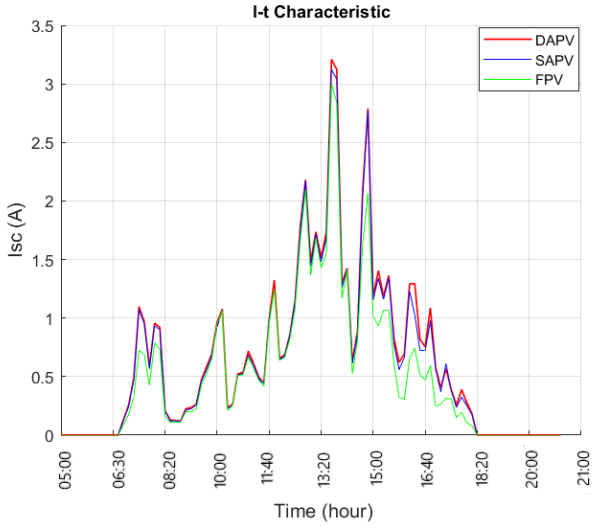

Figure 32. I-t graph plotted on 21st September, 2021.

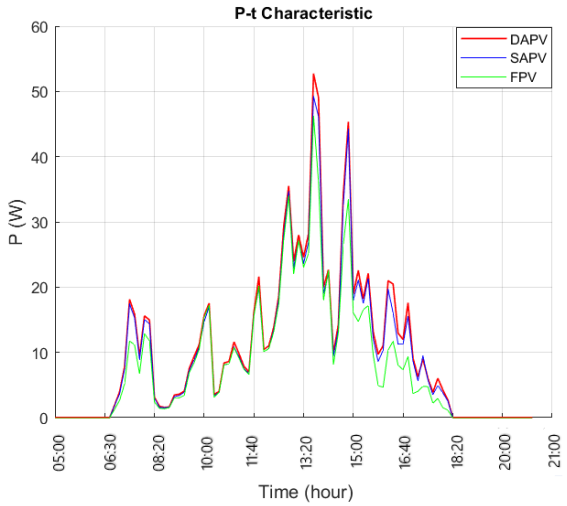

Figure 33. P-t graph plotted on 21st September, 2021.

To compare the energy produced by DAPV, SAPV and FPV, area under Power-time (P-t) curve was calculated. In terms of percentage, the efficiency differences between FPV, DAPV and SAPV were calculated by comparing the energy obtained from PV panels. The formula given below can be used to calculate the efficiency differences and energy output of the DAPV system, SAPV system, and FPV system based on the power curves plotted.

$$W \cong \sum_{i=0}^{n} \frac{y(x_i)+y(x_{i+1})}{2}.h = \frac{h}{2}\sum_{i=0}^{n}(y(x_i) + y(x_{i+1})) \quad (8)$$

Where, number of measurements is denoted by n, and measurement interval in hours is denoted by h. In this study, area under P-t graph was calculated by considering h=0.167 and n=79 in accordance with the graph given in Figure 25. When n equals 79, the value correlates with number of measurements that are taken with intervals of 10 minutes between 06:20 - 19:20 hours. 'h' shows the 10-minute intervals in hours. Other formulas and calculations are given in Appendix A.

The measurement results for 21st of September showed that dual-axis PV panel functions 5.58% and 23.13% (on average) more efficiently as compared to single-axis and fixed PV panels, respectively. It was observed that the single-axis PV panel functions 16.62% (on average) more efficiently than fixed panel. During a total of 61-day period between 1st of August, 2021 and 30th of September, 2021, the weather was sunny for 42 days, cloudy for 11 days and rainy for 8 days. Using the same method described above for the energy calculation of the three example days, the daily amounts of energy production were calculated for a total of 61 days. In Figure. 34, the 61-day energy production amounts of all three panels are given.

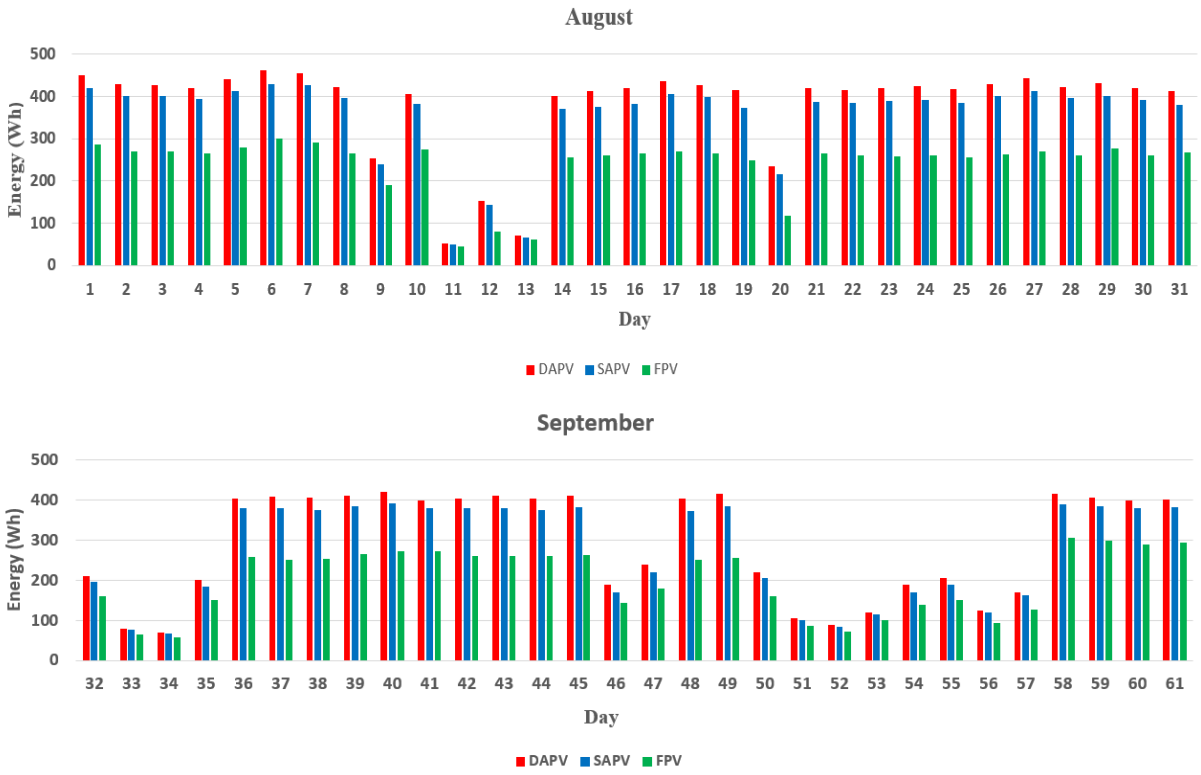

Figure 34. 61-day Energy production amounts.

In Figure 35, energy production amounts of PV panels for sunny, cloudy and rainy days are given separately.

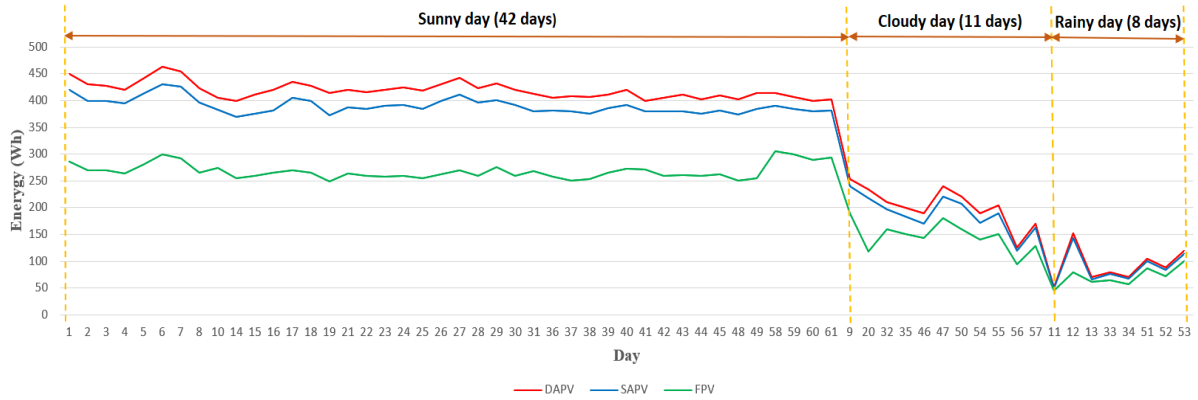

Figure 35. Energy production amounts according to sunny, cloudy and rainy days.

According to the data obtained from the measurements, DAPV produced 419.16 Wh, SAPV produced 390.38 Wh and FPV produced 268.29 Wh on daily average on sunny days. DAPV produced 7.37% more energy than SAPV and 56.23% more energy than FPV, and SAPV produced 45.51% more energy than FPV.

On cloudy days, DAPV produced 203.36 Wh, SAPV produced 189 Wh and FPV produced 146.73 Wh on daily average. On cloudy days, DAPV produced 7.59% more energy than SAPV and 38.59% more than FPV, and SAPV produced 28.81% more energy than FPV.

On rainy days, DAPV produced 92 Wh, SAPV produced 87.38 Wh and FPV produced 71 Wh on daily average. On rainy days, DAPV produced 5.29% more energy than SAPV and 29.58% more energy than FPV, and SAPV produced 23.07% more energy than FPV.

In the 61-day period, DAPV produced 337.34 Wh, SAPV produced 314.32 Wh and FPV produced 220.49 Wh on daily average. On daily average, DAPV produced 7.32% more energy than SAPV and 52.99% more energy than FPV, and SAPV produced 42.55% more energy than FPV.

VI. CONCLUSION

In this study, single-axis STS, double-axis STS, and fixed PV system were designed and controlled in real time. The designed systems were compared based on their efficiencies and power. According to the results of the measurements; on sunny days, DAPV was observed to produce 419.16 Wh, SAPV 390.38 Wh and FPV 268.29 Wh on daily average. According to the results, DAPV produced 7.37% more energy than SAPV and 56.23% more energy than FPV, and SAPV produced 45.51% more energy than FPV. On cloudy days, DAPV was found to produce 203.36 Wh, SAPV 189 Wh and FPV 146.73 Wh on daily average. According to the results, DAPV produced 7.59% more energy than SAPV and 38.59% more energy than FPV, and SAPV produced 28.81% more energy than FPV. DAPV was found to produce 92 Wh, SAPV 87.38 Wh and FPV 71 Wh on daily average on rainy days. According to the results, DAPV produced 5.29% more energy than SAPV and 29.58% more energy than FPV, and SAPV produced 23.07% more energy than FPV. In a total of 61-day period with 42 days of sunshine, 11 days of cloud and 8 days of rain, DAPV was determined to produce 337.34 Wh, SAPV 314.32 Wh and FPV 220.49 Wh on daily average. On daily average, DAPV produced 7.32% more energy than SAPV and 52.99% more energy than FPV, and SAPV produced 42.55% more energy than FPV.

To ensure optimal performance and minimal malfunctioning of STSs, the electrical and mechanical parts, and also the software of the system need to be designed in the most optimal way by taking climatic and geographical conditions into account. In this study, PLC was used as a controller as it is known to be more appropriate for industrial conditions. Worm gear reducers were used in the single-axis STS and dual-axis STS because reducers are able to function with no angle limitations and by reducing rpm, reducers can increase the torque. The choice of stepper motors for the solar tracking system was based on their smooth operation with a PLC and high precision in positioning. The experimental results have revealed that the proposed solar tracking systems work smoothly and efficiently.

The designed system is based on astronomical data (date and time), so it does not experience the instability problem as seen in LDR systems. It provides an advantage in terms of cost and reliability as there is no need for internet and/or GPS connection. The system's reliability is increased with the inclinometer. Once the system is initially set up, it does not require manual alignment. It can operate regardless of the geographical location and weather conditions. The solar tracker based on date and time, which uses reduction gear units to move

simultaneously in both east-west and north-south directions, has advanced accuracy with a tracking error of less than 0.2°, as well as good movement stability, low maintenance cost, and easy installation.

In future researches, the STSs that are installed and controlled based on astronomical data will be compared with several different control methods applied in the literature. Additionally, the tracking systems will be optimized for minimum cost and energy consumption. Finally, it is envisaged that the proposed STSs will be further developed and applied practically on a larger PV system for an institute or a commercial organization.

ACKNOWLEDGMENT

This work was supported by Coordinatorship of Research Projects of the Karabuk University. Project Number: FYL-2020-2191.

REFERENCES

[1] World Energy Data. (2022). Trends of Eneygy Production. https://www.worldenergydata.org/world-electricity-generation/

[2] Republic of Türkiye Energy Market Regulatory Authority. (2024). Electricity Market Sector Report March 2024. https://epdk.gov.tr

[3] Ocłon, P., Cisek, P., Kozak-Jagieła, E., Taler, J., Taler, D., Skrzyniowska, D., &Fedorczak- Cisak, M. (2020). Modeling and experimental validation and thermal performance assessment of a sun-tracked and cooled PVT system under low solar irradiation. *Energy Conversion Management*,222, (113289), 1-23.

[4] Jamroen, C., Fongkerd, C., Krongpha, W., Komkum, P., Pirayawaraporn, A., & Chindakham, N. (2021). A novel UV sensor-based dual-axis solar tracking system: Implementation and performance analysis. *Applied Energy*, 299, (117295), 1-17.

[5] Hafez, A., Yousef, A., & Harag, N. (2018). Solar tracking systems: technologies and trackers drive types – a review. *Renewable and Sustainable Energy Reviews*, 91, 754–782.

[6] Al-Rousan, N., Mat Isa, N.A., & Mat Desa, M.K. (2018). Advances in solar photovoltaic tracking systems: A review. *Renewable and Sustainable Energy Reviews*, 82, 2548–2569.

[7] Awasthi, A., Shukla, A. K., Murali Manohar, S. R., Dondariya, C., Shukla, K. N., Porwal, D., & Richhariya, G. (2020). Review on sun tracking technology in solar PV system. *Energy Reports*, 6, 392–405.

[8] Seme, S., Stumberger, B., Hadziselimovic M., & Sredensek, K. (2020). Solar photovoltaic tracking systems for electricity generation: A review. *Energies*, 13, (4224), 1-24.

[9] Sumathi, V., Jayapragash, R., Bakshi, A., & Akella, P. K. (2017). Solar tracking methods to maximize PV system output – A review of the methods adopted in recent decade. *Renewable and Sustainable Energy Reviews*, 74, 130-138.

[10] Nsengiyumva, W., Chen, S. G., Hu L., & Chen X. (2018). Recent advancements and challenges in solar tracking systems (STS): A review. *Renewable and Sustainable Energy Reviews*, 81, 250–279.

[11] Jamroen, C., Komkum, P., Kohsri, S., Himananto, W., Panupintu, S., & Unkat, S. (2020). A low-cost dual-axis solar tracking system based on digital logic design: Design and implementation. *Sustainable Energy Technologies and Assessments*, 37, (100618), 1-14.

[12] Ali Jallal, M., Chabaa, S., & Zeroual, A. (2020). A novel deep neural network based on randomly occurring distributed delayed PSO algorithm for monitoring the energy produced by four dual-axis solar trackers. *Renewable Energy*, 149, 1182–1196.

[13] Zhu, Y., Liu, J., & Yang, X. (2020). Design and performance analysis of a solar tracking system with a novel single-axis tracking structure to maximize energy collection. *Applied Energy*, 264, (114647), 1-7.

[14] Al-Rousan, N., Mat Isa, N. A., & Mat Desa, M. K. (2020). Efficient single and dual axis solar tracking system controllers based on adaptive neural fuzzy inference system. *Journal of King Saud University - Engineering Sciences*, 32, (7), 459–469.

[15] Lim, B. H., Lim, C. S., Li, H., Hu, X. L., Chong, K. K., Zong, J. L., Kang, K., & Tan, W. C. (2020). Industrial design and implementation of a large-scale dual-axis sun tracker with a vertical-axis-rotating-platform and multiple-row-elevation structures. *Solar Energy*, 199, 596–616.

[16] Okoye, C. O., Bahrami, A., & Atikol, U. (2018). Evaluating the solar resource potential on different tracking surfaces in Nigeria. *Renewable and Sustainable Energy Reviews*, 81, 1569–1581.

[17] Jacobson, M. Z., & Jadhav, V. (2018). World estimates of pv optimal tilt angles and ratios of sunlight incident upon tilted and tracked pv panels relative to horizontal panels. *Solar Energy*,169, 55–66.

[18] Yilmaz, S, Ozcalik, H. R., Dogmus, O., Dincer F., Akgol O., & Karaaslan M. (2015). Design of two axes sun tracking controller with analytically solar radiation calculations. *Renewable and Sustainable Energy Reviews*, 43, 997–1005.

[19] Martín-Martínez S., Cañas-Carretõn M., Honrubia-Escribano A., & Gõmez-Lázaro E. (2019). Performance evaluation of large solar photovoltaic power plants in spain. *Energy Conversion and Management*, 183, 515–528.

[20] Bahrami, A., & Okoye, C. O. (2018). The performance and ranking pattern of pv systems incorporated with solar trackers in the northern hemisphere. *Renewable and Sustainable Energy Reviews*, 97, 138–151.

[21] Bahrami A., Okoye C.O., & Atikol U. (2017). Technical and economic assessment of fixed, single and dual-axis tracking pv panels in low latitude countries. *Renewable Energy*, 113, 563–579.

[22] Antonanzas, J., Urraca, R., Martinez-de Pison, F. J., & Antonanzas F. (2018). Optimal solar tracking strategy to increase irradiance in the plane of array under cloudy conditions: A study across Europe. *Solar Energy*, 163, 122-130.

[23] Fernández-Ahumada L. M., Casares F. J., Ramírez-Faz J., & Lõpez-Luque R. (2017). Mathematical study of the movement of solar tracking systems based on rational models. *Solar Energy*,150, 20-29.

[24] Barker, L., Neber, M., & Lee, H., (2013). Design of a low-profile two-axis solar tracker. *Solar Energy*, 97, 569–576.

[25] Eke, R., Senturk, A., 2012., "Performance comparison of a double-axis sun tracking versus fixed PV system", *Sol. Energy* 86 (9), 2665–2672.

[26] Roth, P., Georgiev, A., & Boudinov, H., (2005). Cheap two axis sun following device", *Energy Conversion Management*, 46, 1179–1192.

[27] Roth, P., Georgiev, A., & Boudinov, H. (2004). Design and construction of a system for suntracking. *Renewable Energy*, 29, 393-402.

[28] Batayneh W., Owais A., & Nairoukh M. (2013). An intelligent fuzzy based tracking controller for a dual-axis solar PV system. *Automation in Constr*uction, 29, 100-106.

[29] Kacira, M., Simsek, M., Babur, Y., & Demirkol, S. (2004). Determining optimum tilt angles and orientations of photovoltaic panels in Sanliurfa, Turkey. *Renewable Energy*, 29, 1265-1275.

[30] Abdallah, K., & Nijmeh S. (2004). Two axes sun tracking system with PLC control. *Energy Conversion and Management*, 45, (11-12), 1931-1939.

[31] Masoumeh, A., Golzarian, M. R., Rohani A., & Zarchi, H. A. (2018). Development of a machine vision dual-axis solar tracking system. *Solar Energy*, 169, 136–143.

[32] Fernandez-Ahumada, L.M., Casares, F.J., Ramírez-Faz, J., & Lopez-Luque, R. (2017). Mathematical study of the movement of solar tracking systems based on rational models. *Solar Energy*, 150, 20-29.

[33] Evseev, E.G., & Kudish, A.I. (2009). The assessment of different models to predict the global solar radiation on a surface tilted to the south. *Solar Energy*, 83, 377-388.

[34] Mousazadeh, H., Keyhani, A., Javadi, A., Mobli, H., Abrinia K., & Sharifi A. (2009). A review of principle and sun-tracking methods for maximizing solar systems output. *Renewabable and Sustainable. Energy Reviews*, 13, (8), 1800-1818.

[35] Lu, H.C., & Shih, T. L. (2010). Fuzzy system control design with application to solar panel active dual-axis Sun tracker system. *Proceeding of the IEEE International Conference on Systems Man and Cybernetics (SMC)*, 10-13 October, İstanbul, 1878-1883.

[36] Rahate, A,, Seung, J., Mehmood, M. U., Kim, Y., Jeon, G., Han, H. J., & Lim, S. H. (2021). Computer vision and photosensor based hybrid control strategy for a two-axis solar tracker - Daylighting application. *Solar Energy*, 224, 175-183.

[37] Wu, C. H., Wang, H. C, & Chang, H. Y. (2022). Dual-axis solar tracker with satellite compass and inclinometer for automatic positioning and tracking. *Energy for Sustainable Development*, 66, 308–318.

[38] Asfaw, A. H. (2023). Manual tracking for solar parabolic concentrator –For the case of solar injera baking, Ethiopia. *Heliyon*, 9, (1), 1-17.

[39] Messenger, R. A., & Ventre, J. (2003). *Photovoltaic systems engineering 2nd ed. CRC Press, Boca Raton*, U.S.A., 437.

[40] Ghassoul, M. (2021). A dual solar tracking system based on a light to frequency converter using a microcontroller. Fuel. Communications 6 (2021) 100007.

[41] Karafil, A., Ozbay, H., Kesler, M., & Parmaksiz, H. (2015). Calculation of optimum fixed tilt angle of PV panels depending on solar angles and comparison of the results with experimental study conducted in summer in Bilecik, Turkey. *2015 9th International Conference on Electrical and Electronics Engineering (ELECO)*, 26-28 November, Bursa, 971-976.

Appendix A

Calculations

$$W_{FPV} \cong \frac{0.167}{2}.\sum_{i=0}^{79}(y(x_i) + y(x_{i+1}) = 3464 \quad (9)$$

$$W_{SAPV} \cong \frac{0.167}{2}.\sum_{i=0}^{79}(y(x_i) + y(x_{i+1}) = 5192 \quad (10)$$

$$W_{DAPV} \cong \frac{0.167}{2}.\sum_{i=0}^{79}(f(x_i) + f(x_{i+1}) = 5550 \quad (11)$$

Using Equations 5-7, the total amount of energy obtained in 13 hours from all the panels were calculated separately. Dividing the total amount of produced energy by total hours, the average amount of energy was obtained. With obtained values, average amount of produced energy per hour was calculated and the results were obtained in terms of kilowatt-hour (kWh) using Equations 12-14 as follows:

$$W_{FPV} = \frac{3464}{13} = 266.46\,Wh = 0.266\,kWh \quad (12)$$

$$W_{SAPV} = \frac{5192}{13} = 399.38\,Wh = 0.399\,kWh \quad (13)$$

$$W_{DAPV} = \frac{5550}{13} = 426.92\,Wh = 0.427\,kWh \quad (14)$$

The average energy produced per hour by FPV is denoted by W_{FPV} and the value is calculated in Equation 12, and the average energy produced per hour by SAPV and DAPV are denoted by W_{SAPV} and W_{DAPV} and the values are calculated in Equations 13 and 14, respectively. The comparison of efficiency percentages (denoted as 'η') of the panels are calculated in Equations 15-17 below.

$$\eta = \frac{W_{DAPV} - W_{FPV}}{W_{FPV}}.100 = \frac{426.92 - 266.46}{266.46}.100 = 60.22\% \quad (15)$$

$$\eta = \frac{W_{DAPV} - W_{SAPV}}{W_{SAPV}}.100 = \frac{426.92 - 399.38}{399.38}.100 = 6.89\% \quad (16)$$

$$\eta = \frac{W_{SAPV} - W_{FPV}}{W_{SFPV}}.100 = \frac{399.38 - 266.46}{266.46}.10049.88\% \quad (17)$$

According to measurement results obtained on 18th of August, dual-axis PV panel was determined to function 6.89% (on average) more efficiently when compared with single-axis PV panel and 60.22% (on average) more efficiently when compared with fixed PV panel. In addition, the single-axis PV panel was observed to function 49.88% (on average) more efficiently than fixed PV panel.

Using formulations given in equations (18-26) similar to equations (9-17), the energy values were calculated for power-time (P-t) graph shown in Fig. 31, in which the measurements were taken on 25th September.

$$W_{FPV} \cong \frac{0.167}{2}.\sum_{i=0}^{66}(y(x_i) + y(x_{i+1}) = 1020 \quad (18)$$

$$W_{SAPV} \cong \frac{0.167}{2}.\sum_{i=0}^{66}(y(x_i) + y(x_{i+1}) = 1296 \quad (19)$$

$$W_{DAPV} \cong \frac{0.167}{2}.\sum_{i=0}^{66}(f(x_i) + f(x_{i+1}) = 1350 \quad (20)$$

$$W_{FPV} = \frac{1020}{10.83333} = 94.15\,Wh = 0.094\,kWh \quad (21)$$

$$W_{SAPV} = \frac{1296}{10.83333} = 119.63\,Wh = 0.12\,kWh \quad (22)$$

$$W_{DAPV} = \frac{1350}{10.83333} = 124.61\,Wh = 0.12\,kWh \quad (23)$$

$$\eta = \frac{W_{DAPV} - W_{FPV}}{W_{FPV}}.100 = \frac{124.61 - 94,15}{94.15}.100 = 32.35\% \quad (24)$$

$$\eta = \frac{W_{DAPV} - W_{SAPV}}{W_{SAPV}}.100 = \frac{124.61 - 119.63}{119.63}.100 = 4.16\% \quad (25)$$

$$\eta = \frac{W_{SAPV} - W_{FPV}}{W_{SFPV}}.100 = \frac{119,63 - 94.15}{94.15}.100 = 27.06\% \quad (26)$$

The measurement results for 25th September showed that dual-axis PV panel functions 4.16% and 32.35% (on average) more efficiently as compared to single-axis and fixed PV panels, respectively. It was observed that the SPV functions 27.06% (on average) more efficiently than FPV.

Using formulations of equations (27-35) similar to equations (18-26), the energy values of FPV, SPV and DPV were calculated for power-time (P-t) graph shown in Fig. 34, in which the measurements were taken on 21st of September.

$$W_{FPV} \cong \frac{0.167}{2}.\sum_{i=0}^{68}(y(x_i)+y(x_{i+1}) = 800 \quad (27)$$

$$W_{SAPV} \cong \frac{0.167}{2}.\sum_{i=0}^{68}(y(x_i)+y(x_{i+1}) = 933 \quad (28)$$

$$W_{DAPV} \cong \frac{0.167}{2}.\sum_{i=0}^{68}(f(x_i)+f(x_{i+1}) = 985 \quad (29$$

$$W_{FPV} = \frac{800}{11.16666} = 71.64\ Wh = 0.072\ kWh \quad (30)$$

$$W_{SAPV} = \frac{933}{11.16666} = 83.55\ Wh = 0.084\ kWh \quad (31)$$

$$W_{DAPV} = \frac{985}{11.16666} = 88.21\ Wh = 0.088\ kWh \quad (32)$$

$$\eta = \frac{W_{DAPV}-W_{FPV}}{W_{FPV}}.100 = \frac{88.21-71.64}{94.1571.64}.100 = 23.13\% \quad (33)$$

$$\eta = \frac{W_{DAPV}-W_{SAPV}}{W_{SAPV}}.100 = \frac{88.21-83.55}{83.55}.100 = 5.58\% \quad (34)$$

$$\eta = \frac{W_{SAPV}-W_{FPV}}{W_{SFPV}}.100 = \frac{83.55-71.64}{71.64}.100 = 16.62\% \quad (35)$$

Appendix B

Part of Ladder Diagram

In this section, a part of the Ladder diagram consisting of a total of 86 networks is given. A total of 8 networks are shown related to driving the stepper motors, taking the values of the angles according to date and time from the data block, measuring the current and voltage of the PV panels, sending the position data to the stepper motor drivers.

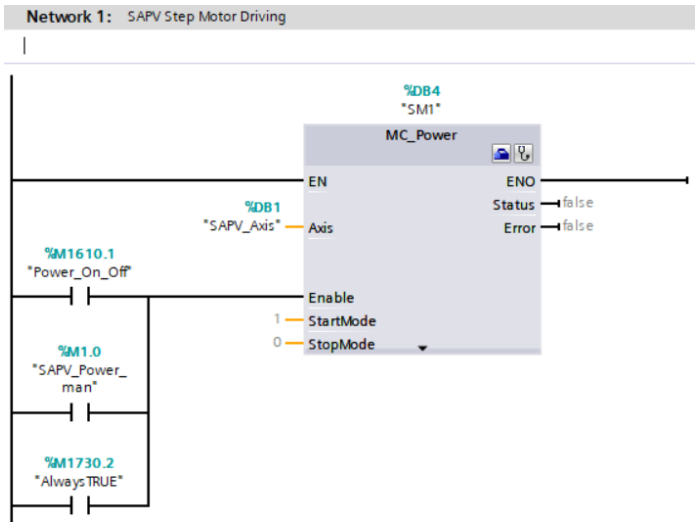

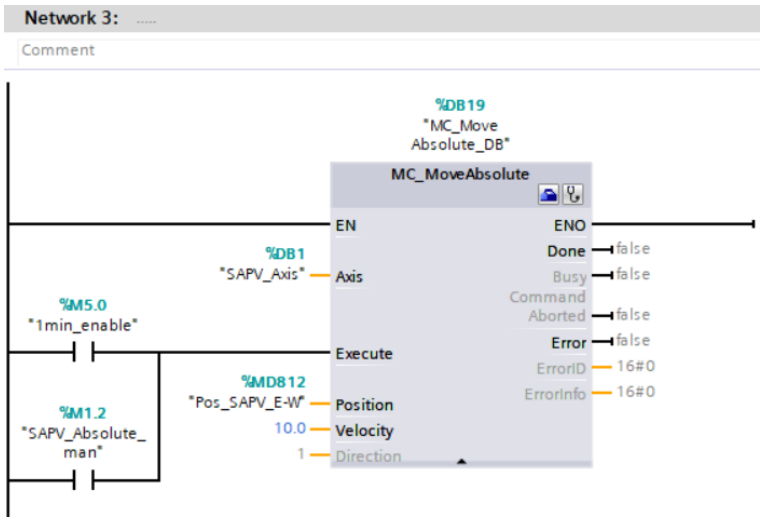
Network 3:
Comment
%DB19
"MC_Move Absolute_DB"
MC_MoveAbsolute
EN
ENO
%DB1
"SAPV_Axis"
Axis
Done
false
Busy
false
Command Aborted
false
Error
false
ErrorID
16#0
ErrorInfo
16#0
%M5.0
"1min_enable"
Execute
%MD812
"Pos_SAPV_E-W"
Position
10.0
Velocity
1
Direction
%M1.2
"SAPV_Absolute_man"

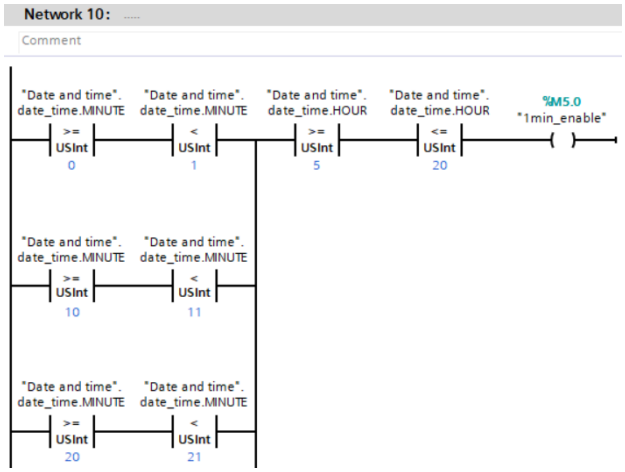
Network 10:
Comment
"Date and time". date_time.MINUTE
>= USInt
0
"Date and time". date_time.MINUTE
< USInt
1
"Date and time". date_time.HOUR
>= USInt
5
"Date and time". date_time.HOUR
<= USInt
20
%M5.0
"1min_enable"
"Date and time". date_time.MINUTE
>= USInt
10
"Date and time". date_time.MINUTE
< USInt
11
"Date and time". date_time.MINUTE
>= USInt
20
"Date and time". date_time.MINUTE
< USInt
21

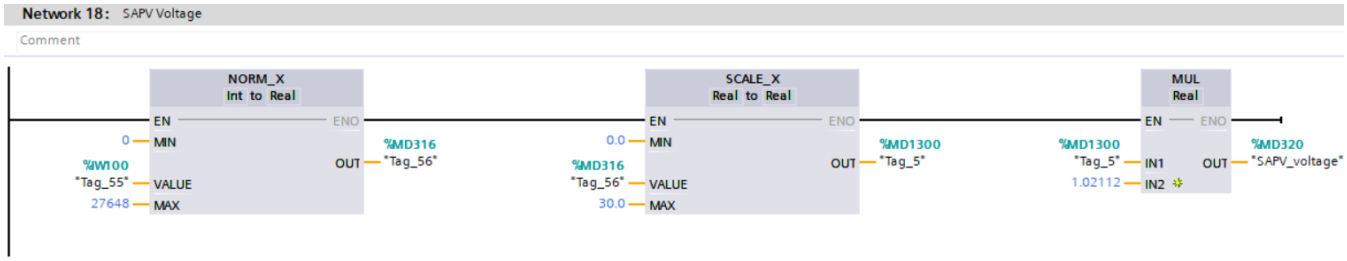
Network 18: SAPV Voltage
Comment
NORM_X
Int to Real
EN
ENO
0
MIN
%W100
"Tag_55"
VALUE
27648
MAX
OUT
%MD316
"Tag_56"
SCALE_X
Real to Real
EN
ENO
0.0
MIN
%MD316
"Tag_56"
VALUE
30.0
MAX
OUT
%MD1300
"Tag_5"
MUL
Real
EN
ENO
%MD1300
"Tag_5"
IN1
1.02112
IN2
OUT
%MD320
"SAPV_voltage"

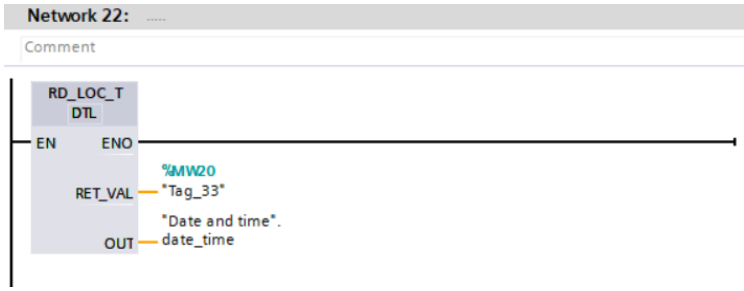
Network 22:
Comment
RD_LOC_T
DTL
EN
ENO
%MW20
"Tag_33"
RET_VAL
"Date and time". date_time
OUT

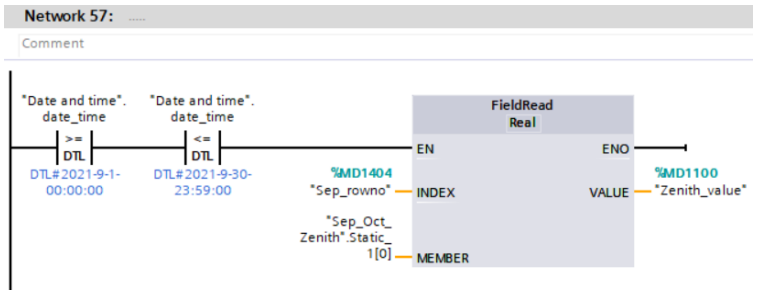
Network 57:
Comment
"Date and time".
date_time
>=
DTL
DTL#2021-9-1-
00:00:00
"Date and time".
date_time
<=
DTL
DTL#2021-9-30-
23:59:00
FieldRead
Real
EN
ENO
%MD1404
"Sep_rowno"
INDEX
VALUE
%MD1100
"Zenith_value"
"Sep_Oct_
Zenith".Static_
1[0]
MEMBER

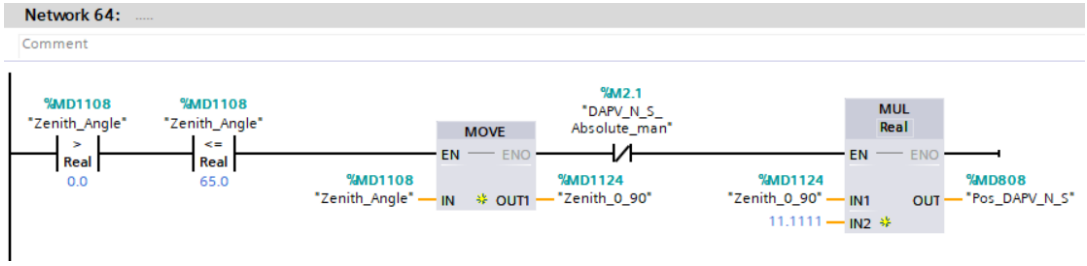
Network 64:
Comment
%MD1108
"Zenith_Angle"
>
Real
0.0
%MD1108
"Zenith_Angle"
<=
Real
65.0
MOVE
EN
ENO
%MD1108
"Zenith_Angle"
IN
OUT1
%MD1124
"Zenith_0_90"
%M2.1
"DAPV_N_S_
Absolute_man"
MUL
Real
EN
ENO
%MD1124
"Zenith_0_90"
IN1
11.1111
IN2
OUT
%MD808
"Pos_DAPV_N_S"